Kinetic modeling of nonequilibrium flow of hard-sphere dense gases

Wei Su [1,2] Livio Gibelli [3] Jun Li [4] Matthew K. Borg [3] and Yonghao Zhang [5,*]

[1]*Division of Emerging Interdisciplinary Areas,*
The Hong Kong University of Science and Technology, Hong Kong, China
[2]*Department of Mathematics, The Hong Kong University of Science and Technology, Hong Kong, China*
[3]*School of Engineering, The University of Edinburgh, Edinburgh EH9 3FB, Scotland, United Kingdom*
[4]*Center for Integrative Petroleum Research, College of Petroleum Engineering and Geosciences,*
King Fahd University of Petroleum and Minerals, Dhahran 31261, Saudi Arabia
[5]*State Key Laboratory of High-Temperature Gas Dynamics, Institute of Mechanics,*
Chinese Academy of Sciences, Beijing 100190, China

A kinetic model is proposed for the nonequilibrium flow of dense gases composed of hard-sphere molecules, which significantly simplifies the collision integral of the Enskog equation using the relaxation-time approach. The model preserves the most important physical properties of high-density gas systems, including the Maxwellian at rest as the equilibrium solution and the equation of state for hard-sphere fluids; all the correct transport coefficients, namely, the shear viscosity, thermal conductivity, and bulk viscosity; and inhomogeneous density distribution in the presence of a solid boundary. The collision operator of the model contains a Shakhov model-like relaxation part and an excess part in low-order spatial derivatives of the macroscopic flow properties; this latter contribution is used to account for the effect arising from the finite size of gas molecules. The density inhomogeneity in the vicinity of a solid boundary in a confined flow is captured by a method based on the density-functional theory. Extensive benchmark tests are performed, including the normal shock structure and the Couette, Fourier, and Poiseuille flow at different reduced densities and Knudsen numbers, where the results are compared with the solutions from the Enskog equation and molecular dynamics simulations. It is shown that the proposed kinetic model provides a fairly accurate description of all these nonequilibrium dense gas flows. Finally, we apply our model to simulate forced wave propagation in a dense gas confined between two plates. The inhomogeneous density near the solid wall is found to enhance the oscillation amplitude, while the presence of bulk viscosity causes stronger attenuation of the sound wave. This shows the importance of a kinetic model to reproduce density inhomogeneity and correct transport coefficients, including bulk viscosity.

I. INTRODUCTION

The Boltzmann equation determines the basic thermofluid properties of gaseous systems composed of a myriad of discrete molecules by providing information on the probability distribution of molecular states at all times. The theory was first developed by Maxwell [1] and Boltzmann [2] and has demonstrated its practical significance since the 1950s last century with the advent of modern aerospace vehicles traveling through the outer atmosphere. The maturation of the theory, especially that the transport coefficients (e.g., shear viscosity, thermal conductivity, and diffusivity) predicted

---

*yonghao.zhang@imech.ac.cn

013401-1

by the Chapman-Enskog expansion of the Boltzmann equation are in good agreement with the experimental data for monatomic gases [3], makes it successful in describing the nonequilibrium gas dynamics encountered in a variety of engineering applications, such as high-altitude flights, nano- and microelectromechanical systems, unconventional natural gas production, vacuum science, and so forth.

However, the Boltzmann equation is only appropriate for dilute gas systems where the intermolecular potential is of a sufficiently short range. So the effective interaction diameter of a molecule approaches zero, while the mean free path of gas molecules remains finite. As such molecular collisions take place, only binary collisions are important, which can be regarded as being localized in the spatial space [4]. However, when the gas is compressed to the level that the interaction diameter and the mean free path become comparable, the effect of the finite size of the interaction diameter should be taken into account; thus, the Boltzmann equation is inaccurate. Meanwhile, the traditional Navier-Stokes equations are also inapplicable due to the shrinking of the flow system size, i.e., the Knudsen number (the ratio of the molecular mean free path to the characteristic flow size) is not small. Such systems can be found in many applications, e.g., high-pressure shock tubes [5], shale gas flows [6–8], gas-liquid mixing in high-pressure injection systems [9], and evaporation and condensation of liquids [10,11].

To describe the gas dynamics at high densities, the Boltzmann equation was first extended by Enskog [12] for rigid spherical molecules. This phenomenological theory, often named the standard Enskog theory, was later modified by van Beijeren and Ernst [13]. The revised Enskog theory was developed to circumvent the defect that, when the original Enskog equation is generalized to model hard-sphere mixtures, it is not consistent with the laws of irreversible thermodynamics. Extension of the Enskog equation was also made for dense granular flows to include inelastic collisions [14–16]. Although it is well known that the Enskog equation for dense gases based on the hard-sphere model may not be able to get accurate transport properties of real fluids, it "provided the first prediction of the transport coefficients of the hard-sphere fluid and opened the way to the calculation of transport properties of real dense fluids" [17]. The Enskog transport theory for hard-sphere fluids can also be extended to real fluids in a simple and straightforward manner to obtain transport coefficients as described in the modified Enskog theory [18]. So the temperature dependence of the collision frequency of a real fluid can be expressed in terms of the equation of state of the real fluid.

Like the Boltzmann equation, numerically solving the Enskog or modified Enskog equations is highly challenging. Both stochastic and deterministic approaches have been developed, including the Monte Carlo quadrature method [19], the direct simulation Monte Carlo (DSMC) method [20,21], and the fast spectral method [6,22]. These methods have been verified through benchmark tests by comparisons with the "exact" molecular dynamics (MD) simulations. Note that another particle method, namely, the consistent Boltzmann algorithm [23], was modified from the DSMC method for the Boltzmann equation by introducing an additional streaming process and an enhanced collision rate. This modification is based on a rather intuitive observation and not directly deduced from the Enskog equation; however, its solutions for large-density flows are comparable to the results of the Enskog equation.

Although accurate results of dense gas flow far from equilibrium can be obtained by solving the Enskog equation, the significant computational costs turn out to be a major constraint, especially for practical applications such as engineering design simulations. Therefore, a computationally efficient kinetic model equation, which replaces the known collision operator of the Enskog equation with a simpler form, is highly desirable. For near-equilibrium states, where the kinetic equation is linearizable, a linear kinetic model can be constructed systematically through approximations to the eigendecomposition of the collision operator [24]. However, in a general nonlinear case, the construction is more arbitrary and phenomenological, depending on the desired mathematical and physical features to preserve [25]. Compared to a dilute gas, one of the major differences in the dynamics of dense gases is that transfer of momentum and energy due to molecular collisions cannot be ignored, which results in the nonzero potential stress tensor and heat flux. As a consequence, not only are the equation of state, shear viscosity, and thermal conductivity modified but also bulk

viscosity comes into play. Besides, when the effect of solid boundary dominates the flow behavior of a tightly confined gas, an inhomogeneous distribution of gas density emerges due to the shield of the solid surface against collisions [26]. Therefore, when developing a kinetic model equation for general nonequilibrium dense gas flows, the following essential criteria need to be satisfied.

(1) The model equation has the unique solution of the Maxwellian at equilibrium and retains the equation of state.

(2) The transport coefficients derived from the model equation are consistent with those obtained from the original kinetic equation; thus, the Navier-Stokes equations at the hydrodynamic limit can be recovered.

(3) The model equation can describe both nonequilibrium and denseness effects, particularly density inhomogeneity, velocity slippage, and temperature jump for the flows in confined space.

A few attempts have been made to develop simplified kinetic models for the Enskog equation. In extending the lattice Boltzmann method to both nonideal gas and liquid flows, Luo [27,28] used the method described in Chapman and Cowling [3] to simplify the Enskog collision integral: the delocalized velocity distribution function of the colliding pair is expanded into a Taylor series of molecular diameter; the zeroth term gives the Boltzmann collision operator, which is replaced by the Bhatnagar-Gross-Krook (BGK) relaxation model [29]; the first-order terms are evaluated by the Maxwellian, resulting in functions of derivatives of macroscopic flow properties including the density, temperature, and bulk velocity, where only the terms involving density are retained; finally all the other higher-order terms are omitted. This lattice Boltzmann model only works for low-speed flows at the hydrodynamic limit. Later, Guo *et al.* [30,31] proposed a simplified kinetic model for strongly inhomogeneous flows, where the density inhomogeneity is taken into account based on the density-functional theory and the Fischer and Methfessel [32] model for inhomogeneous fluids. This model has not properly considered thermal and nonequilibrium effects, its validity being restricted to equilibrium and isothermal flows. For systems far from equilibrium, a kinetic model was developed from the revised Enskog equation [25,33], where the collision operator is first projected into a Hilbert space spanned by the polynomials of the molecular velocity of up to degree 2 and then split into two parts: the collisional transfer contribution to the momentum and energy fluxes, and the remaining part. The former contribution is expressed in terms of the potential stress tensor and heat flux, while a BGK-like relaxation term approximates the latter contribution. Since the potential stress tensor and heat flux are still integral functionals of the colliding velocity distribution functions, this kinetic model is a highly nonlinear integrodifferential equation, which is only applicable to a few simple flows where simplifications can be exploited, e.g., uniform shear flow. Sadr and Gorji [34] derived a cubic Fokker-Planck (FP) model for nonequilibrium dense gas flows, in which an extra advection of the velocity distribution function in the physical space is added to the FP-Boltzmann model to match the potential momentum and heat flux approximated by the Enskog equation. The model was verified by simulating thermal and shear-driven flows under different confinements by comparing the temperature and velocity profiles with the Enskog solutions. Recently, a Shakhov-Enskog kinetic model was proposed by Wang *et al.* [35]. Emphasis was put on capturing the correct shear viscosity, but the recovery of correct thermal conductivity and bulk viscosity was omitted. Furthermore, the gas molecule-surface interactions were not addressed since the model was verified for a normal shock wave structure where the surface effect was absent.

As pointed out above, when simulating general nonequilibrium dense gas flows, none of the present kinetic models can largely simplify the complexity of the Enskog equation and reduce the computational cost while simultaneously satisfying all the aforementioned criteria. Particularly, the inhomogeneous density profile has been overlooked in these models, which, however, is vital to be properly considered as it may influence transport processes. In this paper, we will develop a kinetic model for the Enskog equation, which recovers the correct equation of state and transport coefficients, and captures gas-surface interactions and their effect on gas dynamical behavior.

The remainder of the paper is arranged as follows. Section II presents details of the kinetic modeling, focusing on the equation of state, the transport coefficients, and the modeling of density inhomogeneity for confined flows. The model equation will be verified through a series of

benchmark tests and applied to investigate the sound wave propagation in a confined dense gas in Sec. III, followed by some conclusions in Sec. IV.

II. KINETIC MODELING OF NONEQUILIBRIUM DENSE GAS FLOW

A. The Enskog equation

In gas kinetic theory, the dynamics of a nonuniform gas system is described by the evolution of the one-particle velocity distribution function $f(t, \boldsymbol{x}, \boldsymbol{v})$, defined so that $f d\boldsymbol{x} d\boldsymbol{v}$ gives the number of molecules within an incremental volume element $d\boldsymbol{x} d\boldsymbol{v}$ in the phase space at position $\boldsymbol{x}$, molecular velocity $\boldsymbol{v}$, and time t. With the information of f, some important macroscopic flow properties, including the number density n, bulk velocity $\boldsymbol{U}$, temperature T, as well as the kinetic stress tensor $\boldsymbol{P}_{\mathrm{k}}$ and heat flux $\boldsymbol{Q}_{\mathrm{k}}$, are immediately determined from the velocity moments:

$$n(t, \boldsymbol{x}) = \int f(t, \boldsymbol{x}, \boldsymbol{v}) d\boldsymbol{v},$$

$$n\boldsymbol{U}(t, \boldsymbol{x}) = \int \boldsymbol{v} f(t, \boldsymbol{x}, \boldsymbol{v}) d\boldsymbol{v},$$

$$\frac{3}{2} n k_{\mathrm{B}} T(t, \boldsymbol{x}) = \int \frac{m}{2} C^2 f(t, \boldsymbol{x}, \boldsymbol{v}) d\boldsymbol{v}, \tag{1}$$

$$\boldsymbol{P}_{\mathrm{k}}(t, \boldsymbol{x}) = \int m\boldsymbol{C}\boldsymbol{C} f(t, \boldsymbol{x}, \boldsymbol{v}) d\boldsymbol{v},$$

$$\boldsymbol{Q}_{\mathrm{k}}(t, \boldsymbol{x}) = \int \frac{m}{2} \boldsymbol{C} C^2 f(t, \boldsymbol{x}, \boldsymbol{v}) d\boldsymbol{v},$$

where m is the molecular mass, k_{B} is the Boltzmann constant, and $\boldsymbol{C} = \boldsymbol{v} - \boldsymbol{U}$ is the peculiar velocity, i.e., the deviation of the molecular velocity from the flow velocity. It is worth mentioning that the kinetic stress tensor $\boldsymbol{P}_{\mathrm{k}}$ and heat flux $\boldsymbol{Q}_{\mathrm{k}}$ result from the momentum and energy transport of free molecular motions between collisions. Meanwhile, the transfer of momentum and energy at collisions plays an important role in determining the dynamics of dense gases, which was first modeled by Enskog [12] for hard-sphere molecules.

The governing equation of f is written as [3]

$$\partial_t f + \boldsymbol{v} \cdot \nabla_{\boldsymbol{x}} f + \boldsymbol{F} \cdot \nabla_{\boldsymbol{v}} f = J_{\mathrm{E}}(f, f), \tag{2}$$

where

$$J_{\mathrm{E}}(f, f) = \sigma^2 \iint \boldsymbol{g} \cdot \boldsymbol{k} \{ \chi^{\mathrm{HS}}[\boldsymbol{x}, \boldsymbol{x} + \sigma\boldsymbol{k}|n] f(t, \boldsymbol{x}, \boldsymbol{v}') f(t, \boldsymbol{x} + \sigma\boldsymbol{k}, \boldsymbol{v}_1')$$

$$- \chi^{\mathrm{HS}}[\boldsymbol{x}, \boldsymbol{x} - \sigma\boldsymbol{k}|n] f(t, \boldsymbol{x}, \boldsymbol{v}) f(t, \boldsymbol{x} - \sigma\boldsymbol{k}, \boldsymbol{v}_1) \} d\boldsymbol{k} d\boldsymbol{v}_1. \tag{3}$$

In Eqs (2) and (3), ∇ denotes the vector differential operator; $\boldsymbol{F}$ is an external body force exerted per unit mass of molecules; σ is the effective molecular diameter; $\boldsymbol{g} = \boldsymbol{v}_1 - \boldsymbol{v}$ is the relative velocity of two colliding molecules, with $\boldsymbol{v}$ and $\boldsymbol{v}_1$ being the molecular velocities before collisions and $\boldsymbol{k}$ a unit vector that specifies their relative position at the time of impact; $\boldsymbol{v}'$ and $\boldsymbol{v}_1'$ are the postcollision velocities, related to the precollision ones through $\boldsymbol{v}' = \boldsymbol{v} + \boldsymbol{k}(\boldsymbol{g} \cdot \boldsymbol{k})$ and $\boldsymbol{v}_1' = \boldsymbol{v}_1 - \boldsymbol{k}(\boldsymbol{g} \cdot \boldsymbol{k})$; finally, χ^{HS} is the two-point pair-correlation function (PCF) of a hard-sphere fluid. To be specific, $\chi^{\mathrm{HS}}[\boldsymbol{x}, \boldsymbol{x}_1|n]$ gives the probability to find molecules at $\boldsymbol{x}$ and $\boldsymbol{x}_1$ in a density field $n(t, \boldsymbol{x})$ at equilibrium. The effect of the finite size of molecular diameter σ is reflected in J_E in two ways. First, the centers of the collision pair are separated by a distance σ so that the first molecule (of velocity $\boldsymbol{v}$) is at the point $\boldsymbol{x}$ while the other molecule (of velocity $\boldsymbol{v}_1$) is at the points $\boldsymbol{x} \mp \sigma\boldsymbol{k}$ before and after a collision. Second, the factor χ^{HS} is introduced to take account of the variation of collision frequency; it is equal to unity for a dilute gas and increases with the gas density.

In the standard Enskog theory, χ^{HS} is defined as the PCF in a uniform equilibrium state, χ, evaluated from the local density at the contact point of the collision pair, i.e.,

$$\chi^{\mathrm{HS}}[\boldsymbol{x}, \boldsymbol{x} \pm \sigma \boldsymbol{k}|n] \equiv \chi\big[n\big(\boldsymbol{x} \pm \tfrac{1}{2}\sigma \boldsymbol{k}\big)\big], \tag{4}$$

where χ is related to n through the equation of state, which will be shown later. In a solid-fluid system, the presence of solid surfaces induces a nonuniform density profile and modifies the PCF, which is no longer equal to the local uniform equilibrium PCF [36]. Therefore, in the framework of the revised Enskog theory, χ^{HS} is a functional of the local density, and the functional dependence should be chosen so that the resulting density field has the form required by equilibrium statistical mechanics [37]; particularly, the equation of van Beijeren and Ernst [13] is based on the exact equilibrium PCF. On the other hand, the PCF and density structure in nonuniform equilibrium have been intensively studied. One of the most successful approaches is the density-functional theory, where the exact PCF is approximated to take the form as that of a uniform equilibrium state; however, it is at an average density $\bar{n}$, i.e.,

$$\chi^{\mathrm{HS}}[\boldsymbol{x}, \boldsymbol{x} \pm \sigma \boldsymbol{k}|n] \equiv \chi[\bar{n}(\boldsymbol{x})]. \tag{5}$$

The density profile is obtained by either solving the Born-Green-Yvon equation [32,38] or minimizing the grand canonical free energy functional [39,40]. Since both of the formulations (4) and (5) rely on the PCF in uniform equilibrium states, in the following sections, we will start from the standard Enskog equation to derive the equation of state and transport coefficients in Sec. II B and propose a kinetic model in Sec. II C; finally, inhomogeneity will be modeled in Sec. II D, adopting an argument used in the density-functional theory that the model can be obtained from the one for the standard Enskog equation with the average density.

B. Equation of state and transport coefficients

To derive the equation of state and transport coefficients from the Enskog equation, we multiply Eq. (2) by the collision invariants $\phi = \{m, m\boldsymbol{v}, \tfrac{1}{2}m v^2\}$ and integrate the resulting equations over $\boldsymbol{v}$. The following balance equations for mass, momentum, and energy are eventually obtained:

$$\partial_t \rho + \nabla \cdot (\rho \boldsymbol{U}) = \int m J_{\mathrm{E}} d\boldsymbol{v},$$

$$\partial_t (\rho \boldsymbol{U}) + \nabla \cdot (\rho \boldsymbol{U}\boldsymbol{U}) + \nabla \cdot \boldsymbol{P}_{\mathrm{k}} = \rho \boldsymbol{F} + \int m\boldsymbol{v} J_{\mathrm{E}} d\boldsymbol{v}, \tag{6}$$

$$\partial_t (\rho e) + \nabla \cdot (\rho e \boldsymbol{U}) + \nabla \cdot (\boldsymbol{Q}_{\mathrm{k}} + \boldsymbol{P}_{\mathrm{k}} \cdot \boldsymbol{U}) = \rho \boldsymbol{F} \cdot \boldsymbol{U} + \int \frac{m}{2} v^2 J_{\mathrm{E}} d\boldsymbol{v},$$

where $\rho = mn$ is the mass density and $e = c_v T + \tfrac{1}{2}U^2$ with $c_v = \frac{3k_{\mathrm{B}}}{2m}$ the total energy per unit mass of gas. Unlike the dilute gas, the quantities $\int \phi J_{\mathrm{E}} d\boldsymbol{v}$ do not generally vanish in dense gases: although the total amount of ϕ possessed by the collision pair is conserved, part of this total is transferred across the diameter σ from one molecule to the other at collision due to the non-negligible size of σ. The nonlocal transport terms can be written in divergence form as [26,41]

$$\int m J_{\mathrm{E}} d\boldsymbol{v} = 0,$$

$$\int m\boldsymbol{v} J_{\mathrm{E}} d\boldsymbol{v} = -\nabla \cdot \boldsymbol{P}_{\mathrm{c}}, \tag{7}$$

$$\int \frac{m}{2} v^2 J_{\mathrm{E}} d\boldsymbol{v} = -\nabla \cdot (\boldsymbol{Q}_{\mathrm{c}} + \boldsymbol{P}_{\mathrm{c}} \cdot \boldsymbol{U}),$$

where $\boldsymbol{P}_c$ and $\boldsymbol{Q}_c$ are the potential stress tensor and heat flux, defined by

$$\{\boldsymbol{P}_c, \boldsymbol{Q}_c\} = \frac{\sigma^2}{2} \iiint (\psi' - \psi) \boldsymbol{k} (\boldsymbol{g} \cdot \boldsymbol{k}) \int_0^\sigma \chi \left\{ n \left[\boldsymbol{x} + \left(\alpha - \frac{\sigma}{2} \right) \boldsymbol{k} \right] \right\}$$
$$\times f(t, \boldsymbol{x} + \alpha \boldsymbol{k}, \boldsymbol{v}) f(t, \boldsymbol{x} + \alpha \boldsymbol{k} - \sigma \boldsymbol{k}, \boldsymbol{v}_1) d\alpha d\boldsymbol{v} d\boldsymbol{v}_1 d\boldsymbol{k}. \tag{8}$$

Here $\psi = \{m\boldsymbol{C}, m\boldsymbol{C}^2/2\}$ and ψ' denotes the corresponding postcollision quantities, and α is a dummy variable.

Equations (6) are not closed unless constitutive relations for the stress tensor and heat flux are given. The Chapman-Enskog expansion is the most widely used method to close the equations, where it is assumed that the solution of the velocity distribution function is in the form of an infinite series $f = f^{(0)}[1 + \Phi^{(1)} + \Phi^{(2)} + \cdots]$ with $\{\Phi^{(r)}, r = 1, 2, \ldots\}$ being a small perturbation in the rth order of the Knudsen number; the zeroth-order estimation $f^{(0)}$ is the uniformly steady state taking the Maxwellian distribution $f^{(0)} = nE$ where

$$E = \left(\frac{m}{2\pi k_B T} \right)^{3/2} \exp \left(-\frac{m\boldsymbol{C}^2}{2k_B T} \right). \tag{9}$$

The first-order approximation $f^{(1)} = f^{(0)}[1 + \Phi^{(1)}]$ can be obtained through expanding χ, $f(\boldsymbol{v}_1)$, and $f(\boldsymbol{v}'_1)$ at $\boldsymbol{x}$ into Taylor's series of the diameter σ, and retaining up to the first-order derivatives, substituting $f = f^{(1)}$, and neglecting all the terms of order higher than the first. The kinetic stress tensor and heat flux can then be approximated to the first order of the Knudsen number by taking moments of $f^{(1)}$, giving

$$\boldsymbol{P}_k^{(1)} = n k_B T \boldsymbol{I} - \frac{\mu^*}{\chi} \left(1 + \frac{2}{5} nb\chi \right) 2\boldsymbol{S},$$
$$\boldsymbol{Q}_k^{(1)} = -\frac{\kappa^*}{\chi} \left(1 + \frac{3}{5} nb\chi \right) \nabla T, \tag{10}$$

where $b = \frac{2}{3}\pi\sigma^3$, $\boldsymbol{I}$ is the unit matrix, and $\boldsymbol{S} = \frac{1}{2}\nabla \boldsymbol{U} + \frac{1}{2}(\nabla \boldsymbol{U})^\top - \frac{1}{3}(\nabla \cdot \boldsymbol{U})\boldsymbol{I}$ is the rate-of-stress tensor; μ^* and κ^* are the gas shear viscosity and thermal conductivity at ordinary pressure, which are $\mu^* = \frac{5}{16}(m k_B T/\pi)^{\frac{1}{2}}/\sigma^2$ and $\kappa^* = \frac{15k_B}{4m}\mu^*$ for hard-sphere gases.

The potential stress tensor and heat flux are derived similarly: approximating the integral with respect to α in Eq. (8) by the midpoint quadrature, expanding χ and $f(\boldsymbol{v}_1)$ by Taylor's series, retaining terms up to first order, and evaluating the resultant integrals using $f^{(1)}$; finally, we have [3]

$$\boldsymbol{P}_c^{(1)} = [n^2 b\chi k_B T - \varpi(\nabla \cdot \boldsymbol{U})]\boldsymbol{I} - \left[\frac{\mu^*}{\chi} \left(1 + \frac{2}{5} nb\chi \right) \frac{2}{5} nb\chi + \frac{3}{5}\varpi \right] 2\boldsymbol{S},$$
$$\boldsymbol{Q}_c^{(1)} = -\left[\frac{\kappa^*}{\chi} \left(1 + \frac{3}{5} nb\chi \right) \frac{3}{5} nb\chi + c_v\varpi \right] \nabla T, \tag{11}$$

where $\varpi = \mu^*\chi(nb)^2$. Accordingly, the first-order approximations of the stress tensor and heat flux are sums of the kinetic component (10) and the potential component (11), as

$$\boldsymbol{P}^{(1)} = [(1 + nb\chi)n k_B T - \varpi(\nabla \cdot \boldsymbol{U})]\boldsymbol{I} - \left[\frac{\mu^*}{\chi} \left(1 + \frac{2}{5} nb\chi \right)^2 + \frac{3}{5}\varpi \right] \cdot 2\boldsymbol{S},$$
$$\boldsymbol{Q}^{(1)} = -\left[\frac{\kappa^*}{\chi} \left(1 + \frac{3}{5} nb\chi \right)^2 + c_v\varpi \right] \nabla T. \tag{12}$$

From the above equations, it is found that the equation of thermodynamic pressure of a gas in uniform equilibrium is

$$p = n k_B T (1 + nb\chi). \tag{13}$$

Using the most used Carnahan and Starling [42] equation of state for the hard-sphere fluid

$$\frac{p}{nk_\mathrm{B}T} = \frac{1 + \eta + \eta^2 - \eta^3}{(1 - \eta)^3}, \tag{14}$$

the pair-correlation function is determined as

$$\chi(n) = \frac{1}{2}\frac{2 - \eta}{(1 - \eta)^3}, \tag{15}$$

where $\eta = \frac{\pi}{6}n\sigma^3$ is the reduced density. Note that Eq. (14) retains its accuracy up to the random packing limit $\eta \simeq 0.47$. When the gas is not in a uniform equilibrium, the pressure must increase by an amount of $-\varpi(\nabla \cdot \boldsymbol{U})$. As a consequence, apart from the viscous resistance, there will be a resistance to the contraction or expansion of gases; the parameter ϖ plays the role of the bulk viscosity. Finally, the shear viscosity and thermal conductivity of a rigid-sphere dense gas are given by

$$\mu = \frac{\mu^*}{\chi}\left(1 + \frac{2}{5}nb\chi\right)^2 + \frac{3}{5}\varpi \tag{16}$$

and

$$\kappa = \frac{\kappa^*}{\chi}\left(1 + \frac{3}{5}nb\chi\right)^2 + c_v\varpi, \tag{17}$$

respectively. Compared with dilute gases, not only does the effect of the finite size of molecules modify the equation of state and change the values of shear viscosity and thermal conductivity, but it also gives rise to the second viscosity. It is worthwhile mentioning that the revised Enskog theory of van Beijeren and Ernst [13], when the exact PCF replaces the uniform equilibrium PCF, yields the same transport coefficients at the Navier-Stokes level as the standard Enskog theory.

C. Kinetic model equation for the standard Enskog equation

In this section, we present a model equation to simplify the standard Enskog equation while retaining its essential physics. The physical requirements for the relaxation terms are: (1) the Maxwellian distribution function as the unique solution at equilibrium; (2) the correct equation of state and transport coefficients; and (3) correct mass, momentum, and energy equations at least up to the Navier-Stokes level. It is also required that the model has a simple form, e.g., combinations of polynomials of molecular velocity and some low-order derivatives of macroscopic quantities. Therefore, we propose that our model is read as

$$\partial_t f + \boldsymbol{v} \cdot \nabla_x f + \boldsymbol{F} \cdot \nabla_v f = J_\mathrm{S} + J_\mathrm{K}, \tag{18}$$

where the collision term has a relaxation form with a Shakhov model-like part being

$$J_\mathrm{S} = \frac{nE - f}{\tau} + \frac{E}{\tau}\frac{2m(1 - \mathrm{Pr})}{5(k_\mathrm{B}T)^2}\boldsymbol{Q}_\mathrm{k} \cdot \boldsymbol{C}\left(\frac{m\boldsymbol{C}^2}{2k_\mathrm{B}T} - \frac{5}{2}\right), \tag{19}$$

and an excess part as

$$J_\mathrm{K} = -n^2 b\chi E\left[\boldsymbol{C} \cdot \nabla \ln(n^2 T\chi) + \left(\frac{m\boldsymbol{C}^2}{3k_\mathrm{B}T} - 1\right)(\nabla \cdot \boldsymbol{U})\right]$$
$$+ \nabla \cdot \left[\frac{E}{k_\mathrm{B}T}\varpi(\nabla \cdot \boldsymbol{U})\boldsymbol{C}\left(\frac{m\boldsymbol{C}^2}{2k_\mathrm{B}T} - \frac{3}{2}\right)\right]. \tag{20}$$

Here, $\tau = \mu/n k_B T$ is the relaxation time calculated according to the shear viscosity of a dense gas (16), and the Prandtl number Pr is calculated as

$$\mathrm{Pr} = \frac{2}{3} \frac{\left(1 + \frac{2}{5}nb\chi\right)^2 + \frac{3}{5}(nb\chi)^2}{\left(1 + \frac{3}{5}nb\chi\right)^2 + \frac{2}{5}(nb\chi)^2}, \tag{21}$$

to recover the correct thermal conductivity (17).

The derivation process of our kinetic model is summarized as follows: the delocalized PCF and the velocity distribution function in the original collision integral are expanded using Taylor's theorem at $\boldsymbol{x}$ up to the first order in the molecular diameter σ. The zeroth-order terms are replaced by the Shakhov relaxation model, while the first-order terms are evaluated by replacing the distribution function with the Maxwellian, and only those directly contributing to momentum and energy are retained. The relaxation time and Prandtl number are determined according to the shear viscosity and thermal conductivity for dense gases, and an additional term involving the second derivative of velocity is introduced for the bulk viscosity. It is straightforward to confirm that the kinetic model equation has a unique solution of the local Maxwellian for gases at equilibrium. Meanwhile, in the limit of dilute gas, i.e., $b \to 0$ and $\chi \to 1$, the excess part J_K vanishes, while the shear viscosity μ and the Prandtl number Pr approach to the values of dilute hard-sphere gases, and then the kinetic model regresses to the Shakhov model for the Boltzmann equation.

The excess part in Eq. (20) takes account of the effect of denseness and the collisional contributions in the momentum and energy fluxes. It is shown that the transfer of mass, momentum, and energy generated by the model collision operator satisfies

$$m \int J d\boldsymbol{v} = 0,$$

$$m \int \boldsymbol{v} J d\boldsymbol{v} = -\nabla \cdot \boldsymbol{P}_c = -\nabla \cdot [n^2 b\chi k_B T - \varpi(\nabla \cdot \boldsymbol{U})]\boldsymbol{I}, \tag{22}$$

$$\frac{m}{2} \int v^2 J d\boldsymbol{v} = -\nabla \cdot (\boldsymbol{Q}_c + \boldsymbol{P}_c \cdot \boldsymbol{U}) = -\nabla \cdot [n^2 b\chi k_B T - \varpi(\nabla \cdot \boldsymbol{U})]\boldsymbol{U},$$

where $J = J_S + J_K$. As expected, the collisional mass transfer is nought. The potential stress tensor $\boldsymbol{P}_c = [n^2 b\chi k_B T - \varpi(\nabla \cdot \boldsymbol{U})]\boldsymbol{I}$ and the heat flux $\boldsymbol{Q}_c = 0$ are not completely consistent with the ones from the Enskog equation [see Eq. (11)]. This is because the excess collision part J_K is expressed using a few low-order derivatives, and information contained in higher-order terms is discarded. However, when applying the Chapman-Enskog expansion to the kinetic model (18), we obtain the first-order approximation to the kinetic stress tensor and heat flux as

$$\boldsymbol{P}_k^{(1)} = n k_B T \boldsymbol{I} - 2\mu \boldsymbol{S}, \quad \boldsymbol{Q}_k^{(1)} = -\kappa \nabla T. \tag{23}$$

It is intriguing that the total stress tensor and heat flux are the same as (12). Consequently, the eliminated high-order information in J_K that does not appear in the collisional momentum and energy transfer is recovered in the kinetic transfer of momentum and energy by defining the relaxation time and Prandtl number in J_S from the shear viscosity and thermal conductivity of dense gases, so that the total stress tensor and heat flux obtained by the present kinetic model coincide with those from the Enskog equation at least to the first-order approximation. Therefore, the equation of state and the transport coefficients of the present model are correctly recovered. The primary feature of our model is its inherent simple structure; meanwhile, it preserves some physical properties that are essential for simulating nonequilibrium dense gas flows. Therefore, our model permits one to perform simulations for practical engineering problems that were not possible until now. One limitation is that the collisional fluxes of momentum and energy derived from the model are inconsistent with those from the original Enskog equation beyond the Navier-Stokes level. Since our model is derived from the principle that it could reproduce the correct transport coefficients through the Chapman-Enskog expansion rather than matching the moments of the Enskog collision operator

via Grad's moment method, the 13- and 26-moment equations (the macroscopic equations describe gas flows of moderate Knudsen numbers) obtained from the current model equation are not exactly the same as those from the Enskog equation [43,44]. However, the differences might not be important because the dense gas effect is usually significant at small Knudsen numbers where the correct transport coefficients are more important (e.g., see the numerical results in Sec. III A). The new kinetic model is developed for flows where both the denseness and rarefaction effects appear locally in the flow field, e.g., pore-scale transport of shale gas at high-pressure and high-temperature geoconditions, and molecular transport of surface-confined fluids at the nanoscale. For such flows, the rarefaction can be described by the Shakhov relaxation term J_S, and the denseness could be captured by the excess part J_K.

D. Modeling of confined flows

For confined flows, inhomogeneity in density arises in the vicinity of the solid-gas interface. When the distance of a molecule from the wall is less than σ, a portion of its surface is shielded by the wall against collisions, so the molecule is pushed to the wall. Monte Carlo simulation [36], which provides an insight into the structure of fluids, had shown that the large densities near walls are caused by the fact that the normal motions of the molecules are largely limited.

Numerical experiments show that the kinetic model presented above cannot capture the density inhomogeneity. To circumvent this defect, we follow the method of Guo *et al.* [30], which is inspired by the density-functional theory for inhomogeneous fluids. The key idea is that the excess Helmholtz free energy for an inhomogeneous fluid can be modeled as that of the homogeneous hard-sphere fluid using some form of weighted densities:

$$\overline{n}(\boldsymbol{x}) = \int n(\boldsymbol{x}')\gamma\big(|\boldsymbol{x} - \boldsymbol{x}'|\big)d\boldsymbol{x}', \tag{24}$$

with $\gamma(\boldsymbol{x})$ being a weighting function. As was mentioned above, the PCF is approximated using the average density (5), and the excess part J_K is thus modified as

$$\overline{J}_K = -\overline{n}^2 b\chi(\overline{n})E\left\{\boldsymbol{C} \cdot [2\nabla \ln \overline{n} + \nabla \ln T + \nabla \ln \overline{\chi}] + \left(\frac{m\boldsymbol{C}^2}{3k_BT} - 1\right)(\nabla \cdot \boldsymbol{U})\right\}$$
$$+ \nabla \cdot \left[\frac{E}{k_BT}\varpi(\nabla \cdot \boldsymbol{U})\boldsymbol{C}\left(\frac{m\boldsymbol{C}^2}{2k_BT} - \frac{3}{2}\right)\right], \tag{25}$$

where $\nabla \ln \overline{n}$ and $\nabla \ln \overline{\chi}$ are estimated as

$$\nabla \ln \overline{n} = \frac{120}{\pi \sigma^5} \frac{1}{\overline{n}} \int_{|\boldsymbol{x}'|<\sigma/2} \boldsymbol{x}'\overline{n}\big(\boldsymbol{x} + \boldsymbol{x}'\big)d\boldsymbol{x}',$$
$$\nabla \ln \overline{\chi} = \frac{120}{\pi \sigma^5} \frac{1}{\chi} \int_{|\boldsymbol{x}'|<\sigma/2} \boldsymbol{x}'\chi\big[\overline{n}\big(\boldsymbol{x} + \boldsymbol{x}'\big)\big]d\boldsymbol{x}', \tag{26}$$

to retain the computational stability in case the density significantly varies. Furthermore, the parameters τ, Pr, and ϖ need to be evaluated from the average density, i.e., $\tau(\overline{n})$, $\mathrm{Pr}(\overline{n})$, and $\varpi(\overline{n})$. In this paper, we use the method of Tarazona [39] to obtain the average density, where the weighting function $\gamma(\boldsymbol{x})$ is expressed as a power series of $\overline{n}$. The series is, in practice, truncated after the third term, and the average density is eventually found as the physically appropriate root of the following equation:

$$\overline{n}(\boldsymbol{x}) = \overline{n}_1(\boldsymbol{x}) + \overline{n}_2(\boldsymbol{x})\overline{n}(\boldsymbol{x}) + \overline{n}_3(\boldsymbol{x})\overline{n}(\boldsymbol{x})^2, \tag{27}$$

where

$$\overline{n}_i(\boldsymbol{x}) = \int \gamma_i\big(|\boldsymbol{x} - \boldsymbol{x}'|\big)n\big(\boldsymbol{x}'\big)d\boldsymbol{x}', \quad i = 1, 2, 3, \tag{28}$$

and the density-independent weighting functions γ_i are given as [45]

$$\gamma_1(|\boldsymbol{x}|) = \begin{cases} \frac{3}{4\pi\sigma^3}, & |\boldsymbol{x}| \leqslant \sigma, \\ 0, & |\boldsymbol{x}| > \sigma, \end{cases}$$

$$\gamma_2(|\boldsymbol{x}|) = \begin{cases} 0.475 - 0.648\left(\frac{|\boldsymbol{x}|}{\sigma}\right) + 0.113\left(\frac{|\boldsymbol{x}|}{\sigma}\right)^2, & |\boldsymbol{x}| \leqslant \sigma, \\ 0.288\left(\frac{\sigma}{|\boldsymbol{x}|}\right) - 0.924 + 0.764\left(\frac{|\boldsymbol{x}|}{\sigma}\right) - 0.187\left(\frac{|\boldsymbol{x}|}{\sigma}\right)^2, & \sigma < |\boldsymbol{x}| \leqslant 2\sigma, \\ 0, & |\boldsymbol{x}| > 2\sigma, \end{cases} \qquad (29)$$

$$\gamma_3(|\boldsymbol{x}|) = \begin{cases} \frac{5\pi\sigma^3}{144}\left[6 - 12\left(\frac{|\boldsymbol{x}|}{\sigma}\right) + 5\left(\frac{|\boldsymbol{x}|}{\sigma}\right)^2\right], & |\boldsymbol{x}| \leqslant \sigma, \\ 0, & |\boldsymbol{x}| > \sigma. \end{cases}$$

Together with the Carnahan-Starling pair-correlation function (15), it has been shown that the above modification can recover the equilibrium density distribution of a hard-sphere fluid confined between two planar walls [30,46].

III. RESULTS AND DISCUSSIONS
A. Couette, Fourier, and Poiseuille flows

In this section, we focus on one-dimensional dense gas flows confined between two infinite, parallel, and planar plates perpendicular to the x direction and located at $x = -H/2$ and $H/2$, respectively. The plates are impenetrable; thus, the average number density between the plates

$$n_0 = \frac{1}{H}\int_{-H/2}^{H/2} n(x)dx \qquad (30)$$

remains constant. The fully diffuse scattering of molecules on both the plates is assumed, i.e., the impinging molecules are reemitted according to the Maxwellian $n_w E(T_w, \boldsymbol{U}_w)$, where T_w and $\boldsymbol{U}_w$ are the preassigned wall temperature and velocity, and n_w is determined from the impenetrable condition. The flows are characterized by the reduced density $\eta_0 = \eta(n_0)$ and the confinement ratio $R = H/\sigma$. Note that the Knudsen number becomes known once η_0 and R are provided:

$$\mathrm{Kn} = \frac{\lambda_0}{H} = \frac{1}{6\sqrt{2}}\frac{1}{\eta_0\chi(\eta_0)}\frac{1}{R}, \qquad (31)$$

where $\lambda_0 = 1/\sqrt{2}\pi n_0\sigma^2\chi(\eta_0)$ is the mean free path in hard-sphere dense gases. For the flows considered, the Knudsen number is not negligible; thus, the nonequilibrium effect has equal importance as the effect of denseness. The flows are simulated by solving the proposed kinetic model equation with $\overline{J}_K$ to account for the density inhomogeneity near solid surfaces. The results are compared with the Monte Carlo solutions of the Enskog equation or MD data whenever available.

We first consider a shear-driven and thermal-driven flow to check whether our model can capture the inhomogeneous density and recover correct shear viscosity and thermal conductivity. The shear-driven flow is the Couette flow, in which the plate at $x = -H/2$ moves at a velocity parallel to its plane, $V_1/\sqrt{k_B T_0/m} = -0.5$ with T_0 being the temperature at equilibrium, while the plate at $x = H/2$ moves in the opposite direction with a velocity $V_2/\sqrt{k_B T_0/m} = 0.5$. The thermal-driven flow is the Fourier flow, which develops when the two plates are at rest but kept at different temperatures, namely, T_1 at $x = -H/2$ and T_2 at $x = H/2$; we impose $T_2 = 2T_1$.

The kinetic model equation is solved by the discrete velocity method (DVM), where the molecular velocity space is truncated into the range $[-6\sqrt{2k_B T_0/m}, 6\sqrt{2k_B T_0/m}]^3$ and discretized by 48 nonuniformly distributed points in each direction [47]. Since the gas molecules cannot fully occupy the region less than half of a molecular diameter away from the plates, the effective computational domain is $x \in [-(H-\sigma)/2, (H-\sigma)/2]$, and the boundary condition is applied to the positions $x = \mp(H-\sigma)/2$, respectively. The one-dimensional spatial domain is partitioned by 401 equidistant points; on each discrete point, the spatial derivatives are approximated by the
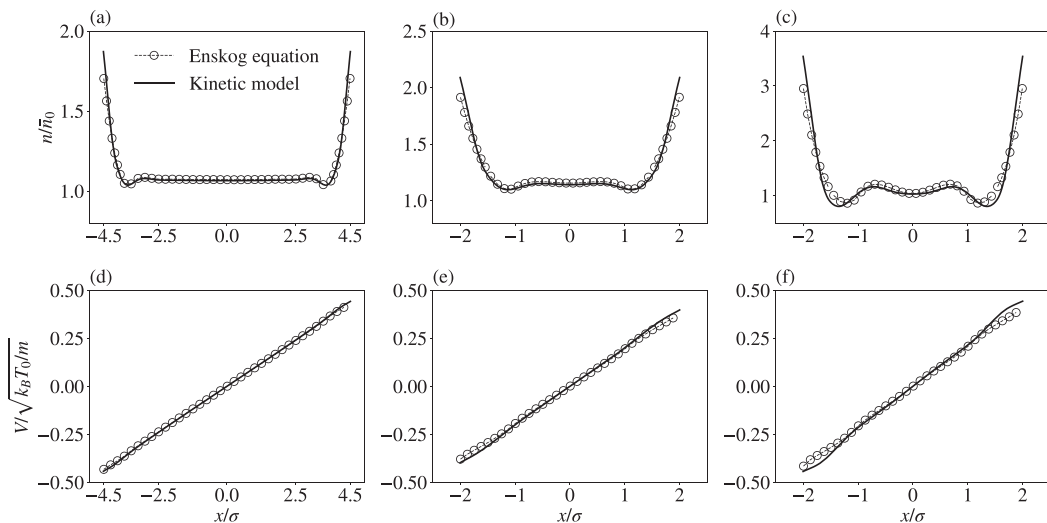
FIG. 1. Profiles of density (first row) and transverse velocity (second row) of the shear driven flow: (a), (d) $\eta_0 = 0.1$, $R = 10$, and Kn = 0.09; (b), (e) $\eta_0 = 0.1$, $R = 5$, and Kn = 0.181; (c), (f) $\eta_0 = 0.2$, $R = 5$, and Kn = 0.067. The solutions to the Enskog equation are represented by empty circles. The DVM solutions of the kinetic model are shown by the solid lines.

second-order finite difference method, while the integral used to evaluate the average density is approximated by the first-order midpoint quadrature. The steady-state solutions are obtained by a semi-implicit iteration scheme [48], where the flow is initialized by the equilibrium state, and the iteration is terminated when the residuals of density, velocity, and temperatures are less than 10^{-6}. The reference solutions are obtained by using a Monte Carlo particle method to solve the Enskog equation [21,26]. In this paper, the computational parameters are as follows: 400 uniform cells are allocated along the x direction, and a total of 200 000 simulating particles are used; the time interval is set as $\Delta t = 10^{-4} \sigma / \sqrt{k_B T_0 / m}$; the steady state is assumed to be reached after 2×10^6 time steps, and another 2×10^6 steps are consumed for sampling to obtain smooth flow profiles.

Figures 1 and 2 show the flow density and transverse velocity and temperature for the Couette flow and Fourier flow, respectively. Different combinations of the reduced densities ($\eta_0 = 0.1$ and 0.2) and confinement factors ($R = 5$ and 10) are considered. The comparisons between the solutions of the Enskog equation and our kinetic model show that our model can capture not only the inhomogeneous structure of the flow density but also the velocity and temperature profiles, although minor discrepancies emerge near the walls when the gas denseness is large at $\eta_0 = 0.2$, and the confinement is extremely tight at $R = 5$.

We then consider the Poiseuille flow driven by an external force F parallel to the plates, which induces a transverse motion of the gas in the direction perpendicular to the x axis. The results obtained from the kinetic model are compared with published MD data [7], where it is assumed that the external force is very small, say $F \ll 2k_B T_0 / mH$. Since the flow is driven by a very small disturbance, the gas system slightly deviates from its equilibrium state, and the kinetic model equation is expressible in a linear form. The formulation of the linearized system can be found in the Appendix, and we focus on the simulation results here. The linearized kinetic model equation is again solved by the DVM. The computational setup is the same as that described above. Figure 3 plots the kinetic results of flow density and velocity for three confinement factors, $R = 10$, 5, and 2, at a reduced density of $\eta_0 = 0.1$, in comparison with the profiles obtained by using event-driven MD. The kinetic solutions are in good agreement with the MD results, and what is noteworthy is that the kinetic model can capture both the density inhomogeneity and slip velocities.
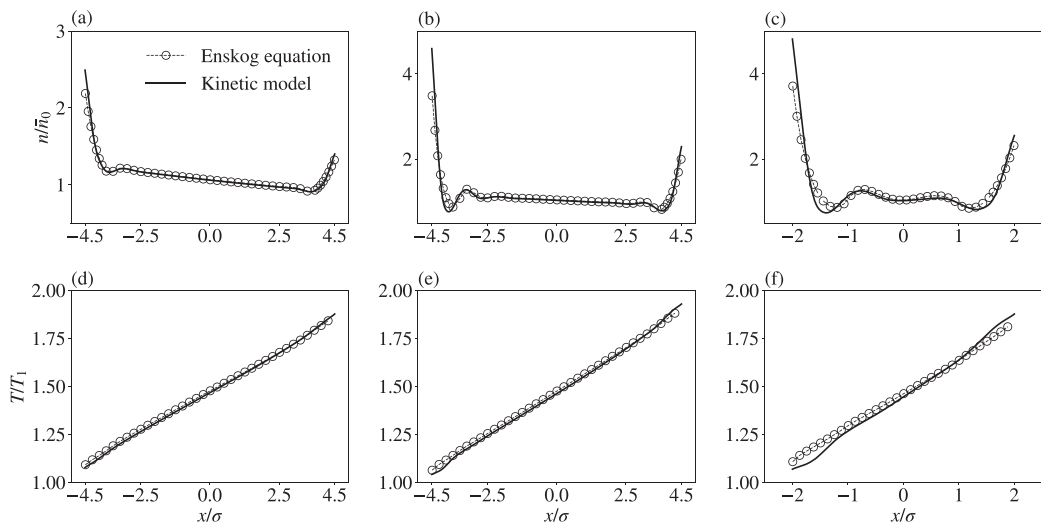
FIG. 2. Profiles of density (first row) and temperature (second row) of the thermally driven flow: (a), (d) $\eta_0 = 0.1$, $R = 10$, and Kn = 0.09; (b), (e) $\eta_0 = 0.2$, $R = 10$, and Kn = 0.034; (c), (f) $\eta_0 = 0.2$, $R = 5$, and Kn = 0.067. The solutions to the Enskog equation are represented by empty circles. The DVM solutions of the kinetic model are shown by the solid lines.

The current kinetic model equation can reasonably describe the flow properties of gas flows with medium denseness. Discrepancy from the Enskog solution becomes noticeable when the reduced density is larger than 0.2 and the confinement ratio is smaller than 5. However, we need to note that the Enskog equation is less accurate at a high denseness, say $\eta = 0.2$ and above, although the
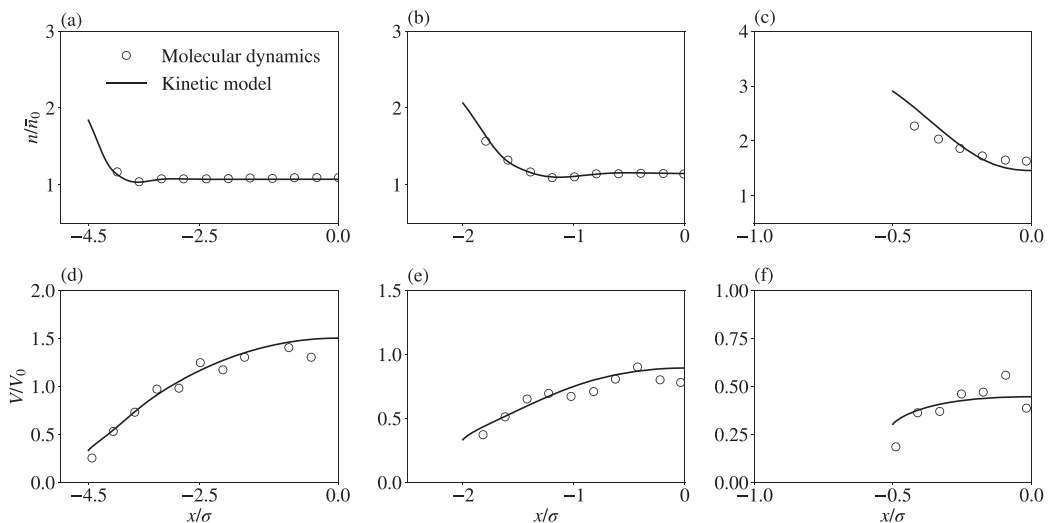

FIG. 3. Profiles of density (first row) and transverse velocity (second row) of the force-driven flow: (a), (d) $\eta_0 = 0.1$, $R = 10$, and Kn = 0.09; (b), (e) $\eta_0 = 0.1$, $R = 5$, and Kn = 0.181; (c), (f) $\eta_0 = 0.1$, $R = 2$, and Kn = 0.452. The results obtained from the event-driven MD simulations are denoted by empty circles. The DVM solutions of the linearized kinetic model are shown by the solid lines. The velocity is normalized by $V_0 = n_0 F H \sqrt{2mk_B T_0}/p_0$. Only half domain $[-H/2, 0]$ is plotted since the flow is symmetric with respect to $x = 0$.

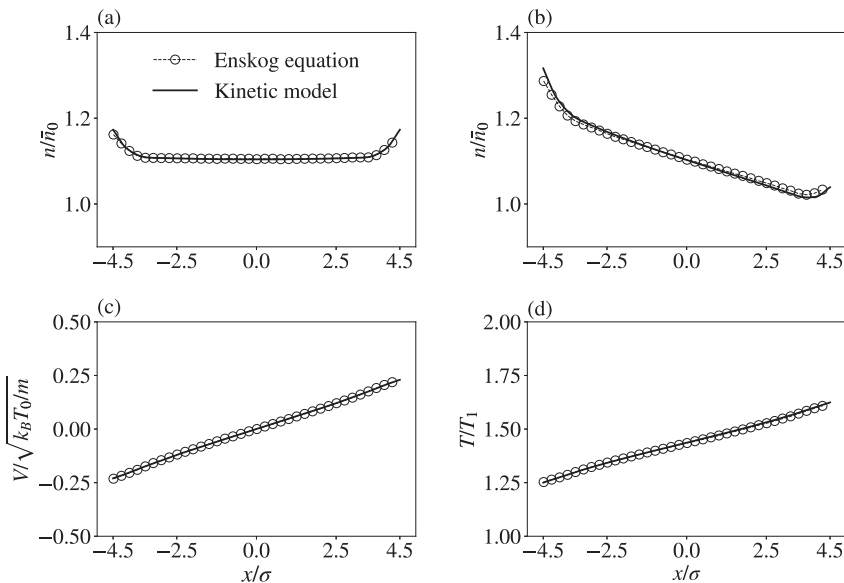FIG. 4. The flows at large Knudsen number: $\eta_0 = 0.01$, $R = 10$, and Kn = 1.149. (a), (c) Profiles of density and transverse velocity of the Couette flow. (b), (d) Profiles of density and temperature for the Fourier flow. The DSMC solutions to the Enskog equation are represented by empty circles. The DVM solutions of the kinetic model are shown by the solid lines.

deviation of the Enskog solution from the MD data at $\eta = 0.2$ is still not large [7]. For the cases calculated, the Knudsen number is relatively low, in $0.05 < \text{Kn} < 0.5$. Large Knudsen number flows occur at a small reduced density and confinement ratio; see Eq. (31). For instance, for $R = 5$ and 10, the Knudsen number is larger than 1 when the reduced density is smaller than 0.02 and 0.01, respectively. Then the excess part of the collision operator is relatively small, and the Shakhov relaxation part largely dominates. Our kinetic model can well capture the Enskog predictions; see Fig. 4.

B. Shock wave structure

In the previous section, we calculate the benchmarking cases of Couette, Fourier, and Poiseuille flows. In each case, the steady flow has no bulk motion, or the direction of its motion is perpendicular to the direction in the gas density varies. Thus, the bulk viscosity does not play an effect. In this section, we use our kinetic model to simulate a normal shock wave in a hard-sphere dense gas to verify the modeling of bulk viscosity and demonstrate its role. When the gas is not stationary, the thermodynamic pressure given by Eq. (13) is increased by an amount of $-\varpi(\nabla \cdot \boldsymbol{U})$; see Eq. (12). According to the mass conservation equation in (6), this term is not zero whenever the gas density varies in the direction of flow motion; it is positive when the gas is contracting and negative when it is expanding. Therefore, the bulk viscosity term represents an additional resistance to contraction or expansion. The value of bulk viscosity approaches zero at the dilute gas limit and becomes large as the degree of denseness intensifies.

In the propagation of a normal shock wave, the boundary effect from solid walls is absent; thus, the kinetic model without modification for density inhomogeneity is solved. The obtained solutions of flow properties are compared to those obtained by solving the Enskog equation. The shock wave structure is characterized by the Mach number and the degree of denseness; the latter can be described by the reduced density η. For comparison, the present kinetic model and the Enskog equation are both solved by the DVM on a one-dimensional spatial domain
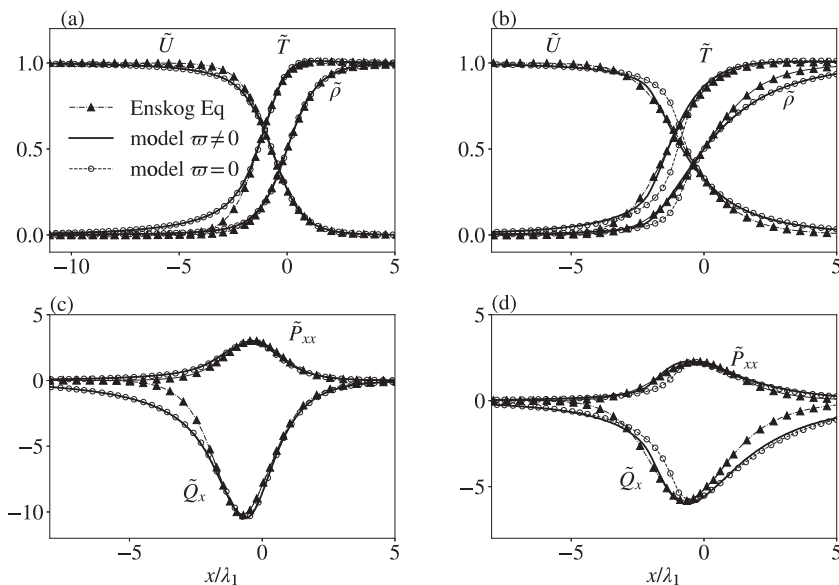
FIG. 5. Profiles of normalized flow properties for a shock wave of Mach number $Ma = 4$: (a), (c) $\eta_1 = 0.022$ and (b), (d) $\eta_1 = 0.077$. The normalized properties are density $\tilde{\rho} = \frac{\rho - \rho_1}{\rho_2 - \rho_1}$, temperature $\tilde{T} = \frac{T - T_1}{T_2 - T_1}$, velocity $\tilde{U} = \frac{U - U_1}{U_2 - U_1}$, total normal stress $\tilde{P}_{xx} = \frac{P_{xx} - p}{\rho_1 k_B T_1 / m}$, and total heat flux $\tilde{Q}_x = \frac{Q_x}{\rho_1 k_B T_1 / m \sqrt{2 k_B T_1 / m}}$.

$x = [-25\lambda_1, 25\lambda_1]$; here, λ_1 is the mean free path based on the upstream equilibrium state, denoted as $\{\rho_1, T_1, U_1\}$, which is related to the downstream equilibrium state $\{\rho_2, T_2, U_2\}$ through the Rankine-Hugoniot relation for dense gases [19]. The molecular velocity space is truncated into the range $[-15\sqrt{2k_B T_1/m}, 15\sqrt{2k_B T_1/m}]^3$ and discretized by 64 equidistant points in each direction. The spatial derivatives are approximated either by the fourth-order discontinuous Galerkin method [48] on 128 uniform elements (in solving the kinetic model) or by the second-order upwind finite difference method on 200 equidistant points (in solving the Enskog equation). A semi-implicit time iterative scheme [48] is applied to seek the steady shock structure, where the flow is initialized by the upstream state in the region of $x < 0$ and the downstream state in $x \geqslant 0$, and the iteration is terminated when the residuals of density, velocity, and temperatures are less than 10^{-6}. For the Enskog equation, the full collision integral is evaluated by the fast spectral method [6,22]. Note that the accuracy of the Enskog equation in simulating the normal shock wave has been verified in several works [35,49] by comparing with the "exact" shock profiles obtained from MD simulations.

Figure 5 plots the profiles of normalized flow properties of a shock wave at the Mach number $Ma = 4$, including the mass density, temperature, velocity, normal stress, and heat flux. The stress and heat flux contain both kinetic and potential contributions. It is found that when the degree of denseness is relatively small with $\eta_1 = 0.022$, the results obtained from the kinetic model with ($\varpi \neq 0$) and without ($\varpi = 0$) the bulk viscosity term are not distinguishable because the value of the bulk viscosity is very small [see Figs. 5(a) and 5(c)]. Notably, the results are in good agreement with those of the Enskog equation. The earlier rises of the temperature and heat flux predicted by the kinetic model are a consequence of the molecular-velocity-independent relaxation time adopted in J_S; the same discrepancies are also observed in the case of a dilute gas solved by the Shakhov model [50]. When we increase the gas denseness to $\eta_1 = 0.077$, the effect of the bulk viscosity becomes noticeable. The variations of the flow properties are steeper if the bulk viscosity is disregarded, especially in front of the shock, which is not unexpected. Indeed, the bulk viscosity makes the shock profile thicker because of more significant resistance to compression. Overall, it is found that only the model with the correct bulk viscosity can accurately match the Enskog predictions.
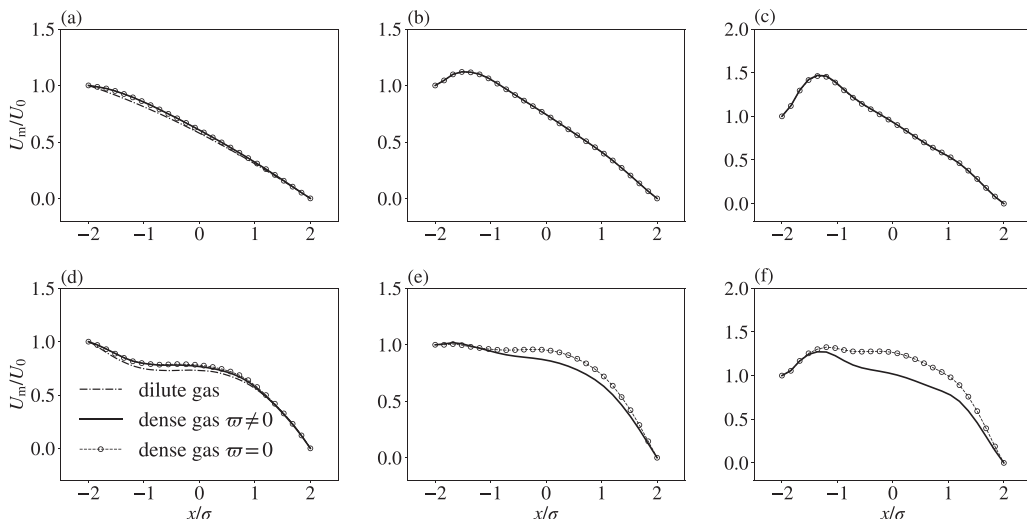
FIG. 6. Profiles of velocity amplitude for the sound wave propagation in the confinement of $R = 5$. The first row shows the results at St $= 1$, and the second row shows those at St $= 5$: (a), (d) $\eta_0 = 0.01$ and Kn $= 2.299$; (b), (e) $\eta_0 = 0.05$ and Kn $= 0.415$; (c), (f) $\eta_0 = 0.1$ and Kn $= 0.181$. The solutions of the linearized kinetic model with and without bulk viscosity are obtained by the DVM. The results for the sound wave in a dilute gas at the same Knudsen number and Strouhal number are included in (a) and (d), which are obtained by solving the Shakhov model equation.

C. Sound wave propagation

The sound wave propagation through a dilute gas confined in macro- and nanochannels has been intensively investigated [51–53]. However, to the best of the authors' knowledge, the one in a tightly confined dense gas has not been studied yet. Investigation of the acoustic and damping properties in dense gases is useful in developing micromachined sensors for supercritical fluids, e.g., the acoustic resonator for detecting density fluctuations in supercritical carbon dioxide [54]. Therefore, it is very intriguing to unravel acoustic characteristics of sound wave propagation in dense gas, especially when the density inhomogeneity and bulk viscosity may have significant effects. We now apply our model to investigate this problem. The flow is generated by the plates at $x = -H/2$ oscillating harmonically in the x direction with a frequency ω so that its velocity depends on time as

$$U_{\text{w}}(t) = U_0 \cos(\omega t), \tag{32}$$

where U_0 is the velocity amplitude, assumed to be very small compared to the most probable molecular velocity $v_{\text{m}} = \sqrt{2k_B T_0/m}$, i.e., $U_0 \ll v_{\text{m}}$. The plate at $x = H/2$ is stationary, which can be treated as a sound receptor. In addition to the reduced density η_0 and confinement ratio R, the flow is defined by the Strouhal number, i.e., the dimensionless oscillating frequency

$$\text{St} = \frac{\omega H}{v_{\text{m}}}. \tag{33}$$

We are interested in the flow state when the oscillation has been fully established so that the periodic flow has the same frequency as the oscillating plate, and the time-dependent problem can be converted into a quasisteady one by introducing complex numbers (see the Appendix). We use the flow velocity, which has the following form,

$$U(t, x) = U_{\text{m}}(x) \cos(\omega t + \varphi_u), \tag{34}$$

to demonstrate the acoustic properties. U_{m} is the velocity amplitude, and φ_u is the velocity phase.
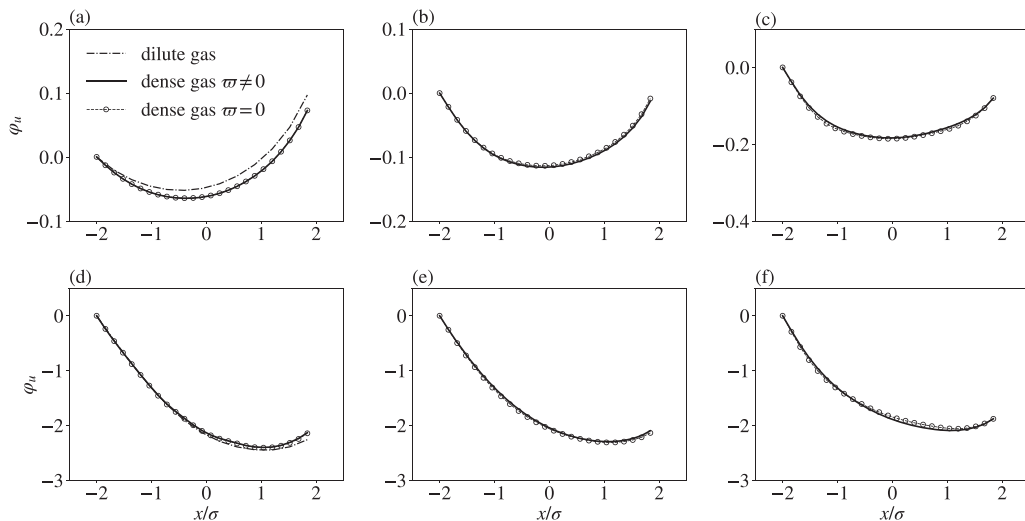
FIG. 7. Profiles of velocity phase for the sound wave propagation in the confinement of $R = 5$. The first row shows the results at St $= 1$, and the second row shows those at St $= 5$: (a), (d) $\eta_0 = 0.01$ and Kn $= 2.299$; (b), (e) $\eta_0 = 0.05$ and Kn $= 0.415$; (c), (f) $\eta_0 = 0.1$, $R = 2$, and Kn $= 0.181$. The solutions of the linearized kinetic model with and without bulk viscosity are obtained by the DVM. The results for the sound wave in a dilute gas at the same Knudsen number and Strouhal number are included in (a) and (d), which are obtained by solving the Shakhov model equation.

Figure 6 illustrates the distribution of the velocity amplitude for the sound wave confined between the plates of $R = 5$ with $\eta_0 = 0.01$, 0.05, and 0.1, respectively. The oscillating frequency is set to be St $= 1$ or 5. The distribution of the velocity phase is plotted in Fig. 7. The comparison between the results of the kinetic model with and without bulk viscosity can reveal the influence of bulk viscosity. Note that in the plots for the flows of $\eta = 0.01$, the solutions of the Shakhov model are added, which stand for the sound wave propagation in a dilute gas at the same Knudsen number and Strouhal number. It is found that when both the degree of denseness and oscillating frequency are small, i.e., $\eta_0 = 0.01$ and St $= 1$, the velocity magnitude monotonously decreases from U_0 at the oscillating plate to zero at the stationary one; when the frequency increases to St $= 5$, the amplitude first decreases followed by a small rise before eventually falling to zero; the influence of the bulk viscosity is negligible, and the profile for dense gases is close to that of a dilute gas, indicating a weak denseness effect. For both St $= 1$ and 5 when η_0 increases to 0.05, a distinct increment in the amplitude is apparent near the oscillating wall, which is more pronounced when η_0 increases to 0.1. Actually, the location of the amplitude peak coincides with that of the first trough in the density profile; see Fig. 1(b) (note that the density profile of the current problem induced by small disturbance coincides with the one when the plates do not move in the x direction). Therefore, the density inhomogeneity results in enhanced oscillations. The influence of bulk viscosity becomes more significant when the oscillating frequency and degree of denseness become large: the amplitude with nonzero bulk viscosity is smaller than that with zero bulk viscosity, and denser gas of larger bulk viscosity will dampen the transport of sound waves more strongly. For all the considered conditions, the velocity phases are a convex function, and the location of the minimum values moves towards the stationary plate when the Strouhal increases from 1 to 5. For St $= 1$, the magnitude of the phase increases with the reduced density; therefore, the enhanced denseness makes the phase lag more severe. For St $= 5$, the trend becomes more complicated. In the region near the oscillating plate $[-(H - \sigma)/2, -H/5]$, the magnitude phase becomes larger with η_0, but outside this region it decreases when η_0 increases. The obtained velocity phases with zero

or nonzero bulk viscosity are almost the same; therefore, the bulk viscosity rarely has any influence on phase shift.

IV. CONCLUSIONS

We have developed a kinetic model to simplify the Enskog equation for the nonequilibrium confined flow of hard-sphere dense gases. The collision operator of the kinetic model contains a relaxation part and an excess part which is a function of low-order spatial derivatives of flow properties, i.e., density, velocity, and temperature, allowing one to take into account the denseness effect. In the dilute limit, the excess part vanishes, and the model regresses to the Shakhov equation. The present model equation can reproduce the equation of state and transport coefficients, including shear viscosity, thermal conductivity, and bulk viscosity of the Enskog equation; thus, the continuum equations of mass, momentum, and energy derived from the kinetic model equation by the first-order Chapman-Enskog expansion are the same as those obtained from the Enskog equation. The density inhomogeneity in the vicinity of a solid boundary is captured by a method inspired by the density-functional theory and Fischer-Methfessel model for inhomogeneous fluids, where the flow density, pair-correlation function, and their spatial derivatives entering the collision operator are replaced by some average quantities.

The numerical results for the normal shock wave, Couette flow, Fourier flow, and Poiseuille flow are in good agreement with the solutions of the Enskog equation, suggesting at least in the range of the flow parameters examined that our kinetic model can capture the effects of denseness, density inhomogeneity, and nonequilibrium. The present kinetic model is then applied to investigate the sound wave propagation in a dense gas confined between two parallel plates. It is found that the density inhomogeneity enhances the velocity amplitude in the region near the oscillating wall, whereas the presence of bulk viscosity strongly dampens the sound wave.

The most attractive feature of the present kinetic model, just like any Boltzmann model equation, is that it largely reduces the computational complexity and cost. Evaluation of the collision operator of the kinetic model requires regular discretization for up to second-order spatial derivatives, which is much simpler than the scheme for evaluating the full collision integral, e.g., the fast spectral method [6,22]. The latter requires transformation between the velocity space and frequency domain and interpolation in the physical space. Furthermore, the simplified model equation allows for reducing the three-dimensional molecular velocity space into a lower-dimensional one when simulating one- or two-dimensional flows. This can significantly reduce memory consumption and computational time in the DVM simulations. For example, the velocity space has been projected into the one-dimensional (for Fourier flow and sound wave propagation) or two-dimensional spaces (for Couette and Poiseuille flows) in this paper, and all the results are obtained within several seconds using a single processor. Therefore, the present kinetic model can strike a balance between modeling accuracy and computational efficiency to enable practical design simulations of nonequilibrium dense gas flows in confined geometries.

APPENDIX: LINEARIZED KINETIC MODEL EQUATION FOR CONFINED DENSE GAS FLOW

Here, we give the formulations of the linearized governing equation system for confined flows that slightly deviate from the equilibrium state. The velocity distribution function is expressed as

$$f(t, x, \boldsymbol{v}) = \tilde{n}_{\text{eq}}(\tilde{x}) E_0(\tilde{\boldsymbol{v}})[1 + h(\tilde{t}, \tilde{x}, \tilde{\boldsymbol{v}})] \frac{n_0}{v_{\text{m}}^3}, \tag{A1}$$

where n_0 is a reference number density, and $v_{\mathrm{m}} = \sqrt{2k_{\mathrm{B}}T_0/m}$ is the most probable molecular velocity with T_0 the equilibrium temperature; $\tilde{n}_{\mathrm{eq}}$ is the dimensionless number density at equilibrium; $\tilde{t} = tv_{\mathrm{m}}/H$, $\tilde{\boldsymbol{x}} = \boldsymbol{x}/H$, and $\tilde{\boldsymbol{v}} = \boldsymbol{v}/v_{\mathrm{m}}$ are the dimensionless time, spatial position, and molecular velocity, respectively; $E_0 = v_{\mathrm{m}}^3 E(\boldsymbol{U} = 0, T = T_0)$ is the dimensionless global Maxwellian with unit density; finally h is the perturbed velocity distribution function, satisfying $|h| \ll 1$. Note that, unlike the dilute gas for which the equilibrium density remains constant, $\tilde{n}_{\mathrm{eq}}(\tilde{\boldsymbol{x}})$ varies with respect to the spatial position and the variation is not a small quantity, especially in the vicinity of solid walls. The macroscopic quantities of interest are defined as

$$\varrho(\tilde{t}, \tilde{\boldsymbol{x}}) = \int E_0(\tilde{\boldsymbol{v}})h(\tilde{t}, \tilde{\boldsymbol{x}}, \tilde{\boldsymbol{v}})d\tilde{\boldsymbol{v}},$$

$$\tilde{\boldsymbol{U}}(\tilde{t}, \tilde{\boldsymbol{x}}) = \int \tilde{\boldsymbol{v}}E_0(\tilde{\boldsymbol{v}})h(\tilde{t}, \tilde{\boldsymbol{x}}, \tilde{\boldsymbol{v}})d\tilde{\boldsymbol{v}},$$

$$\theta(\tilde{t}, \tilde{\boldsymbol{x}}) = \int \left(\frac{2}{3}\tilde{\boldsymbol{v}}^2 - 1\right)E_0(\tilde{\boldsymbol{v}})h(\tilde{t}, \tilde{\boldsymbol{x}}, \tilde{\boldsymbol{v}})d\tilde{\boldsymbol{v}}, \tag{A2}$$

$$\tilde{\boldsymbol{P}}(\tilde{t}, \tilde{\boldsymbol{x}}) = \int 2\tilde{\boldsymbol{v}}\tilde{\boldsymbol{v}}E_0(\tilde{\boldsymbol{v}})h(\tilde{t}, \tilde{\boldsymbol{x}}, \tilde{\boldsymbol{v}})d\tilde{\boldsymbol{v}},$$

$$\tilde{\boldsymbol{Q}}(\tilde{t}, \tilde{\boldsymbol{x}}) = \int \tilde{\boldsymbol{v}}\left(\tilde{\boldsymbol{v}}^2 - \frac{5}{2}\right)E_0(\tilde{\boldsymbol{v}})h(\tilde{t}, \tilde{\boldsymbol{x}}, \tilde{\boldsymbol{v}})d\tilde{\boldsymbol{v}},$$

where ϱ and θ are the perturbed density and temperature satisfying $n/n_0 = \tilde{n}_{\mathrm{eq}}(1 + \varrho)$ and $T/T_0 = 1 + \theta$, respectively; and $\tilde{\boldsymbol{U}} = \boldsymbol{U}/v_{\mathrm{m}}$, $\tilde{\boldsymbol{P}} = \boldsymbol{P}_{\mathrm{k}}/n_0\tilde{n}_{\mathrm{eq}}k_{\mathrm{B}}T_0$ as well as $\tilde{\boldsymbol{Q}} = \boldsymbol{Q}_{\mathrm{k}}/n_0\tilde{n}_{\mathrm{eq}}v_{\mathrm{m}}$ are the dimensionless flow velocity, stress tensor, and heat flux, respectively. Furthermore, the external force, relaxation time, and bulk viscosity are normalized as $\tilde{\boldsymbol{F}} = \boldsymbol{F}v_{\mathrm{m}}^2/H$, $\tilde{\tau} = \tau v_{\mathrm{m}}/H$, and $\tilde{\varpi} = \varpi v_{\mathrm{m}}/n_0k_{\mathrm{B}}T_0H$, respectively. In the remainder of the Appendix, the tilde can be omitted without causing any confusion. The linearized kinetic model equation for the perturbed velocity distribution function h is then written as

$$\partial_t h + \boldsymbol{v} \cdot \nabla h + \nabla \ln n_{\mathrm{eq}} \cdot \boldsymbol{v}h = 2\boldsymbol{F} \cdot \boldsymbol{v} + \frac{\overline{n}_{\mathrm{eq}}}{\tau_{\mathrm{eq}}}\left[\mathcal{L} + \frac{4}{5}(1 - \mathrm{Pr}_{\mathrm{eq}})\boldsymbol{Q} \cdot \boldsymbol{v}\left(\boldsymbol{v}^2 - \frac{5}{2}\right) - h\right]$$

$$- \frac{\overline{n}_{\mathrm{eq}}^2}{n_{\mathrm{eq}}}b\overline{\chi_{\mathrm{eq}}}(\mathcal{L}\boldsymbol{v} - \boldsymbol{U}) \cdot (2\nabla \ln \overline{n}_{\mathrm{eq}} + \nabla \ln \overline{\chi}_{\mathrm{eq}})$$

$$- \frac{\overline{n}_{\mathrm{eq}}^2}{n_{\mathrm{eq}}}b\overline{\chi_{\mathrm{eq}}}\left[\boldsymbol{v} \cdot (\nabla\varrho + \nabla\theta) + \left(\frac{2}{3}\boldsymbol{v}^2 - 1\right)(\nabla \cdot \boldsymbol{U})\right]$$

$$+ \frac{1}{n_{\mathrm{eq}}}\boldsymbol{v}\left(\boldsymbol{v}^2 - \frac{3}{2}\right) \cdot \nabla[\varpi_{\mathrm{eq}}(\nabla \cdot \boldsymbol{U})], \tag{A3}$$

where

$$\mathcal{L} = \varrho + 2\boldsymbol{U} \cdot \boldsymbol{v} + \theta\left(\boldsymbol{v}^2 - \tfrac{3}{2}\right), \tag{A4}$$

and $\overline{\chi}_{\mathrm{eq}} = \chi(\overline{n}_{\mathrm{eq}})$, while $\overline{n}_{\mathrm{eq}}$, $\nabla \ln \overline{n}_{\mathrm{eq}}$, and $\nabla \ln \overline{\chi}_{\mathrm{eq}}$ are the average quantities in Eqs. (24) and (26) evaluated around the local equilibrium density n_{eq}. The transport coefficients are also evaluated from $\overline{n}_{\mathrm{eq}}$. The left-hand side of the above equation shows that the transport of h in the spatial space contains two parts: the variation of the equilibrium density n_{eq} and the variation h itself. Before applying some discretization schemes to solve the equation (A3), its nonlinear version (18) is solved under the constrain of equilibrium to obtain n_{eq}; then the linear equation is solved with n_{eq} as known quantity to obtain the other flow properties.

When considering the problem of sound propagation, it is assumed that the periodic flow state has been fully established so that all the time-dependent quantities oscillate at the same frequency

as the wall. To improve numerical efficiency, we eliminate the time variable by including an explicit time-varying term $\exp(i\mathrm{St}t)$, where i is the imaginary unit. The time-dependent quantities are then expressed as $M(t) = \mathrm{Re}\{\hat{M}\exp(i\mathrm{St}t)\}$ with M being either of $\{h, \varrho, \theta, \boldsymbol{U}, \boldsymbol{P}, \boldsymbol{Q}\}$ and $\mathrm{Re}\{\cdot\}$ denoting the real part of a complex number. The governing equation is the same as (A3), but the time-dependent variables are replaced by $\hat{M}$ and the time derivative ∂_t is replaced by $i\mathrm{St}$. Therefore, the problem is converted into a quasisteady one.

[1] J. C. Maxwell, IV. On the dynamical theory of gases, Phil. Trans. R. Soc. London **157**, 49 (1867).

[2] L. Boltzmann, Weitere Studien über das Wärmegleichgewicht unter Gasmolekülen, *Kinetische Theorie II: Irreversible Prozesse Einführung und Originaltexte* (Vieweg+Teubner, Verlag, Wiesbaden, 1970), pp. 115–225.

[3] S. Chapman and T. G. Cowling, *The Mathematical Theory of Non-Uniform Gases: An Account of the Kinetic Theory of Viscosity, Thermal Conduction and Diffusion in Gases*, Cambridge Mathematical Library (Cambridge University, New York, 1990).

[4] S. Harris, *An Introduction to the Theory of the Boltzmann Equation* (Holt, Rinehart and Winston, New York, 1971).

[5] E. L. Peterson and R. K. Hanson, Nonideal effects behind reflected shock waves in a high-pressure shock tube, Shock Waves **10**, 405 (2001).

[6] L. Wu, H. Liu, J. M. Reese, and Y. H. Zhang, Non-equilibrium dynamics of dense gas under tight confinement, J. Fluid Mech. **794**, 252 (2016).

[7] Q. Sheng, L. Gibelli, J. Li, M. K. Borg, and Y. H. Zhang, Dense gas flow simulations in ultra-tight confinement, Phys. Fluids **32**, 092003 (2020).

[8] B. Shan, R. Wang, Z. Guo, and P. Wang, Contribution quantification of nanoscale gas transport in shale based on strongly inhomogeneous kinetic model, Energy **228**, 120545 (2021).

[9] R. N. Dahms and J. C. Oefelein, Non-equilibrium gas–liquid interface dynamics in high-pressure liquid injection systems, Proc. Combust. Inst. **35**, 1587 (2015).

[10] A. Frezzotti, L. Gibelli, and S. Lorenzani, Mean field kinetic theory description of evaporation of a fluid into vacuum, Phys. Fluids **17**, 012102 (2005).

[11] M. Kon, K. Kobayashi, and M. Watanabe, Method of determining kinetic boundary conditions in net evaporation/condensation, Phys. Fluids **26**, 072003 (2014).

[12] D. Enskog, *Kinetische Theorie der Wärmeleitung, Reibung und Selbstdiffusion in Gewissen Verdichteten Gasen und Flüssigkeiten*, Kungl. Svenska vetenskapsakademiens handlingar (Almqvist & Wiksells boktryckeri-a.-b., 1922).

[13] H. Van Beijeren and M. Ernst, The modified Enskog equation, Physica **68**, 437 (1973).

[14] J. T. Jenkins and S. B. Savage, A theory for the rapid flow of identical, smooth, nearly elastic, spherical particles, J. Fluid Mech. **130**, 187 (1983).

[15] C. K. K. Lun, S. B. Savage, D. J. Jeffrey, and N. Chepurniy, Kinetic theories for granular flow: inelastic particles in couette flow and slightly inelastic particles in a general flowfield, J. Fluid Mech. **140**, 223 (1984).

[16] M. J. Esteban and B. Perthame, On the modified Enskog equation for elastic and inelastic collisions. Models with spin, Annales de l'I.H.P. Analyse non linéaire **8**, 289 (1991).

[17] S. Bastea, Transport properties of dense fluid argon, Phys. Rev. E **68**, 031204 (2003).

[18] H. J. M. Hanley, R. D. McCarty, and E. G. D. Cohen, Analysis of the transport coefficients for simple dense fluids: Application of the modified Enskog theory, Physica **60**, 322 (1972).

[19] A. Frezzotti and C. Sgarra, Numerical analysis of a shock-wave solution of the Enskog equation obtained via a Monte Carlo method, J. Stat. Phys. **73**, 193 (1993).

[20] J. M. Montanero and A. Santos, Simulation of the Enskog equation à la Bird, Phys. Fluids **9**, 2057 (1997).

[21] A. Frezzotti, A particle scheme for the numerical solution of the Enskog equation, Phys. Fluids **9**, 1329 (1997).

[22] L. Wu, Y. H. Zhang, and J. M. Reese, Fast spectral solution of the generalized Enskog equation for dense gases, J. Comput. Phys. **303**, 66 (2015).

[23] F. J. Alexander, A. L. Garcia, and B. J. Alder, A Consistent Boltzmann Algorithm, Phys. Rev. Lett. **74**, 5212 (1995).

[24] E. P. Gross and E. A. Jackson, Kinetic models and the linearized Boltzmann equation, Phys. Fluids **2**, 432 (1959).

[25] A. Santos, J. M. Montanero, J. W. Dufty, and J. J. Brey, Kinetic model for the hard-sphere fluid and solid, Phys. Rev. E **57**, 1644 (1998).

[26] A. Frezzotti, Monte Carlo simulation of the heat flow in a dense hard sphere gas, Eur. J. Mech. B Fluids **18**, 103 (1999).

[27] L.-S. Luo, Unified Theory of Lattice Boltzmann Models for Nonideal Gases, Phys. Rev. Lett. **81**, 1618 (1998).

[28] L.-S. Luo, Theory of the lattice Boltzmann method: Lattice Boltzmann models for nonideal gases, Phys. Rev. E **62**, 4982 (2000).

[29] P. L. Bhatnagar, E. P. Gross, and M. Krook, A model for collision processes in gases. I. Small amplitude processes in charged and neutral one-component systems, Phys. Rev. **94**, 511 (1954).

[30] Z. Guo, T. S. Zhao, and Y. Shi, Simple kinetic model for fluid flows in the nanometer scale, Phys. Rev. E **71**, 035301(R) (2005).

[31] Z. Guo, T. S. Zhao, and Y. Shi, Generalized hydrodynamic model for fluid flows: From nanoscale to macroscale, Phys. Fluids **18**, 067107 (2006).

[32] J. Fischer and M. Methfessel, Born-Green-Yvon approach to the local densities of a fluid at interfaces, Phys. Rev. A **22**, 2836 (1980).

[33] J. W. Dufty, A. Santos, and J. J. Brey, Practical Kinetic Model for Hard Sphere Dynamics, Phys. Rev. Lett. **77**, 1270 (1996).

[34] M. Sadr and M. H. Gorji, A continuous stochastic model for non-equilibrium dense gases, Phys. Fluids **29**, 122007 (2017).

[35] P. Wang, L. Wu, M. T. Ho, J. Li, Z.-H. Li, and Y. H. Zhang, The kinetic Shakhov-Enskog model for non-equilibrium flow of dense gases, J. Fluid Mech. **883**, A48 (2020).

[36] I. K. Snook and D. Henderson, Monte Carlo study of a hard–sphere fluid near a hard wall, J. Chem. Phys. **68**, 2134 (1978).

[37] H. van Beijeren, Equilibrium Distribution of Hard-Sphere Systems and Revised Enskog Theory, Phys. Rev. Lett. **51**, 1503 (1983).

[38] J. Fischer and U. Heinbuch, Relationship between free energy density functional, Born-Green-Yvon, and potential distribution approaches for inhomogeneous fluids, J. Chem. Phys. **88**, 1909 (1988).

[39] P. Tarazona, Free-energy density functional for hard spheres, Phys. Rev. A **31**, 2672 (1985).

[40] B. Götzelmann and S. Dietrich, Pair correlation function of inhomogeneous hard sphere fluids, Fluid Phase Equilib. **150-151**, 565 (1998).

[41] C. Cercignani and M. Lampis, On the kinetic theory of a dense gas of rough spheres, J. Stat. Phys. **53**, 655 (1988).

[42] N. F. Carnahan and K. E. Starling, Equation of state for nonattracting rigid spheres, J. Chem. Phys. **51**, 635 (1969).

[43] G. M. Kremer and E. Rosa, On Enskog's dense gas theoirt. I. The method of moments for monatomic gases, J. Chem. Phys. **89**, 3240 (1988)

[44] H. Struchtrup and A. Frezzotti, Twenty-six moment equations for the Enskog-Vlasov equation, J. Fluid Mech. **940**, A40 (2022)

[45] T. K. Vanderlick, L. E. Scriven, and H. T. Davis, Molecular theories of confined fluids, J. Chem. Phys. **90**, 2422 (1989).

[46] Z. Guo, T. S. Zhao, and Y. Shi, Temperature dependence of the velocity boundary condition for nanoscale fluid flows, Phys. Rev. E **72**, 036301 (2005).

[47] W. Su, S. Lindsay, H. Liu, and L. Wu, Comparative study of the discrete velocity and lattice Boltzmann methods for rarefied gas flows through irregular channels, Phys. Rev. E **96**, 023309 (2017).

[48] W. Su, P. Wang, Y. H. Zhang, and L. Wu, Implicit discontinuous Galerkin method for the Boltzmann equation, J. Sci. Comput. **82**, 39 (2020).

[49] A. Frezzotti, Molecular dynamics and Enskog theory calculation of shock profiles in a dense hard sphere gas, Comput. Math. Appl. **35**, 103 (1998).

[50] L. Wu, C. White, T. J. Scanlon, J. M. Reese, and Y. H. Zhang, A kinetic model of the Boltzmann equation for non-vibrating polyatomic gases, J. Fluid Mech. **763**, 24 (2015).

[51] N. G. Hadjiconstantinou and A. L. Garcia, Molecular simulations of sound wave propagation in simple gases, Phys. Fluids **13**, 1040 (2001).

[52] D. Kalempa and F. Sharipov, Sound propagation through a rarefied gas confined between source and receptor at arbitrary Knudsen number and sound frequency, Phys. Fluids **21**, 103601 (2009).

[53] R. Wang and K. Xu, The study of sound wave propagation in rarefied gases using unified gas-kinetic scheme, Acta Mech. Sin. **28**, 1022 (2012).

[54] S. Kakio, K. Hayashi, E. Kondoh, and Y. Nakagawa, Behavior of surface acoustic wave resonators in supercritical CO_2, Jpn. J. Appl. Phys. **50**, 07HD08 (2011).